

Lead isotope analysis of marine carbonates and seawater by multiple collector ICP-MS

Matthew K. Reuer^{a,*}, Edward A. Boyle^{b,1}, Barry C. Grant^{b,1}

^aMIT/WHOI Joint Program in Oceanography, Massachusetts Institute of Technology, Cambridge, MA 02139, USA

^bDepartment of Earth, Atmospheric, and Planetary Sciences, E34-200, Massachusetts Institute of Technology, Cambridge, MA 02139, USA

Received 31 July 2002; accepted 30 April 2003

Abstract

A consistent method for stable lead isotope analysis of marine carbonates and seawater is presented, utilizing multiple collector ICP-MS (MC-ICP-MS). This study presents new observations of the large ($0.7\% \text{ amu}^{-1}$), time-dependent mass bias determined by thallium normalization, including preferential light ion transmission induced by the acceleration potential and plasma interface ($\beta = -1.3$ to 0.9). These experiments show equivalent results for three empirical correction laws, and the previously proposed $\beta_{\text{Pb}}/\beta_{\text{Tl}}$ correction does not improve isotope ratio accuracy under these conditions. External normalization to SRM-981 following the thallium correction provides one simple alternative, and a rationale is provided based on secondary bias effects. With current intensities less than 1.5×10^{-12} A, external isotope ratio precision better than 250 ppm for SRM-981 $^{207}\text{Pb}/^{206}\text{Pb}$ and $^{208}\text{Pb}/^{206}\text{Pb}$ ratios is observed (2σ). From reconstructed lead isotopic variability in the North Atlantic, this instrumental precision results in a signal-to-noise ratio greater than 100. Matrix effects are significant with concomitant calcium in SRM-981 (-280 ppm at $257 \mu\text{M} [\text{Ca}]$). With the appropriate corrections and minimal concomitants, MC-ICP-MS can reliably determine $^{207}\text{Pb}/^{206}\text{Pb}$ and $^{208}\text{Pb}/^{206}\text{Pb}$ ratios of marine carbonates (30 mg) and seawater (160–200 g).

© 2003 Elsevier B.V. All rights reserved.

Keywords: Stable isotopes; Lead isotope ratios; Inductively coupled plasma methods; $^{207}\text{Pb}/^{206}\text{Pb}$; $^{208}\text{Pb}/^{206}\text{Pb}$

1. Introduction

Isotope ratio analysis by multiple collector ICP-MS (MC-ICP-MS) is a promising mass spectrometric technique, and its merits are well established for geochemistry (see reviews by Walder, 1997; Halliday et al., 2000). Previous studies have addressed lead isotope analysis of NIST standard reference materials

and standard rock digests (Walder and Freedman, 1992; Hirata, 1996; Belshaw et al., 1998; Rehkämper and Halliday, 1998; White et al., 2000; Thirlwall, 2001, 2002), examining how mass bias, normalization techniques, and sample matrices affect isotope ratio precision and accuracy. Here several new observations are provided for $^{207}\text{Pb}/^{206}\text{Pb}$ and $^{208}\text{Pb}/^{206}\text{Pb}$ analyses of marine carbonate and seawater samples. The described method accommodates small sample lead masses (3–6 ng), exhibits favorable precision (<250 ppm, 2σ), and provides a consistent and rapid technique for this environmental tracer.

* Corresponding author. Fax: +1-609-258-1724.

E-mail addresses: mreuer@princeton.edu (M.K. Reuer), eaboyle@mit.edu (E.A. Boyle), barryg@mit.edu (B.C. Grant).

¹ Fax: +1-617-253-8630.

The analytical context for this method should first be considered. The utility of lead isotopes as an anthropogenic tracer was established by Chow and co-workers (Chow and Johnstone, 1965; Chow and Earl, 1970, 1972; Chow et al., 1973, 1975). These studies demonstrated systematic, global-scale isotopic variability among leaded gasoline, coal, and aerosol samples. For example, a 14% range in leaded gasoline $^{206}\text{Pb}/^{207}\text{Pb}$ was observed between Bangkok, Thailand (1.072), and Santiago, Chile (1.238, Chow et al., 1975). The unique isotopic composition of multiple anthropogenic sources has provided new constraints on heavy metal provenance in modern atmospheric, terrestrial, and marine systems (e.g., Flegal et al., 1986; Sturges and Barrie, 1987; Church et al., 1990; Véron et al., 1994; Hamelin et al., 1997; Alleman et al., 1999; Bollhöfer and Rosman, 2001). Lead isotope time series recovered from ice cores (Rosman et al., 1993; Rosman et al., 2000), peat records (Shotyk et al., 1998; Weiss et al., 1999), lake sediment records (Graney et al., 1995), and surface corals (Shen and Boyle, 1987) have also demonstrated significant time-dependent isotopic variability. Two common characteristics of anthropogenic lead isotope analysis are thus low concentrations within complex natural matrices and a large isotopic range.

A second consideration is the difference between MC-ICP-MS and established thermal ionization mass spectrometric (TIMS) techniques. The established advantages of MC-ICP-MS include the ionization of most elements within the inductively coupled plasma (e.g., Fe and Hf) and the introduction of various sample types at atmospheric pressure (e.g., solutions, ablated aerosols, or chromatography isolates). For stable lead isotopes, the principal advantages are greater sample throughput ($n=4-5\text{ h}^{-1}$) and fewer preparative steps. This study addresses the possible analytical artifacts pertinent to marine carbonates and seawater and provides the associated isotope ratio precision and accuracy for the Micromass IsoProbe MC-ICP-MS.

2. Methods

Sample preparation followed standard laboratory protocols for trace element analysis, including acid, reagent, and plasticware preparation under Class 100

conditions. Here the specific protocols for lead isotope analysis of seawater and surface corals are briefly described.

2.1. Surface coral and seawater sample preparation

Surface coral samples collected from North Rock, Bermuda ($32^{\circ}29'\text{N}$, $64^{\circ}48'\text{W}$), were cleaned using a modified technique of Shen and Boyle (1988a), removing contaminant organic or oxide phases from the coral aragonite lattice. The modifications to this method include: (1) the use of two rather than three cleaning sequences on coarse aragonite fragments and the 280–700 μm size fraction; and (2) the extension of each oxidative ($\text{NaOH}-\text{H}_2\text{O}_2$) and reducing (citric acid–hydrazine) cleaning cycle from 10 to 30 min. The isotopic composition of occluded contaminants does not equal the aragonite lead, creating significant, nonsystematic biases if they are not removed from the aragonite lattice. The success of the cleaning technique was determined for each sample by replicate Pb/Ca analysis of homogenized splits, utilizing isotope dilution ICP-MS and flame AAS at MIT (VG Plasmaquad 2⁺). The isotope dilution method included direct analysis of dissolved, diluted coral, adding a gravimetrically calibrated ^{204}Pb spike (Oak Ridge National Laboratory) to all samples. Where Pb/Ca replicates did not agree to 2 nmol/mol, samples were reprocessed and reanalyzed, only measuring the isotopic composition of adequately cleaned samples.

Replicate sample analyses cannot eliminate possible elemental or isotopic biases introduced by evenly distributed contaminants not removed by the cleaning process. Two observations, however, suggest this error might be small. First, coral–seawater partition coefficients ($D_p=[X/\text{Ca}^{2+}]_{\text{coral}}/[X/\text{Ca}^{2+}]_{\text{seawater}}$, where X denotes the chemical species of interest) for most elements are close to unity, suggesting minor preferential uptake or exclusion of CaCO_3 substituents and low residual contamination (Reuer et al., 2003). Second, isotopic agreement is observed between 1981 coral and 1982 seawater $^{206}\text{Pb}/^{207}\text{Pb}$ and $^{208}\text{Pb}/^{207}\text{Pb}$ from Bermuda, with a $^{206}\text{Pb}/^{207}\text{Pb}$ offset of 250 ppm (see below). Both field and culture calibration studies are required to best address this issue, but preliminary observations suggest residual contaminant biases are minor relative to the environmental variability.

Moderate volume seawater samples were prepared by the $\text{Mg}(\text{OH})_2$ coprecipitation method (Wu and Boyle, 1997b; Weiss et al., 2000). Larger sample volumes were required (160–240 ml)² relative to elemental analysis (1200 μl) given the necessary counting statistics, Faraday cup noise, and low seawater lead concentrations (Wu and Boyle, 1997a). Surface samples were collected with established procedures, including underway sampling with the towed fish technique (see Vink et al., 2000), pole sampling with a polycarbonate bottle clamp, and vane sampling. Hydrocasts utilized the MITESS automated trace element sampler described in Dickey et al. (1998). Seawater lead was preconcentrated by excess $\text{Mg}(\text{OH})_2$ coprecipitation, adding 400 μl of vapor-distilled ammonia to each 40 ml subsample, mixing the precipitate by shaking and inversion, and separating the $\text{Mg}(\text{OH})_2$ (s) by centrifugation. Dissolved aragonite and seawater $\text{Mg}(\text{OH})_2$ (s) concentrates were reduced to dryness in 3-ml Savillex PFTE beakers and redissolved in 400- μl 1.1 N HBr (Seastar).

Lead separation from the sample matrix included established anion exchange techniques described by Kraus and Moore (1953) and Strelow (1978). Mini-columns (75 μl) were constructed from Teflon shrink tubing (4:1 shrink ratio, 9.53 mm, Texloc) and Teflon supports. Eichrom AG-1X8 (chloride form, 200–400 mesh) anion exchange resin was utilized, cleaned for 7 days in triple-distilled 6.0 N HCl with continuous agitation. Before use, the resin was rinsed $20 \times$ in $d\text{H}_2\text{O}$ and sized by gravitational settling, retaining the intermediate fraction. The loaded resin slurry was then cleaned with 1000- μl 6.0 N HCl and converted to the bromide form with 400- μl 1.1 N HBr. The major cations were eluted with 400- μl 1.1 N HBr, complexing sample lead as PbBr_4^{2-} . The resin was converted to the chloride form with 200- μl 2.0 N HCl, and the sample was eluted with 500- μl 6.0 N HCl. Quantitative lead recoveries were observed from the column separation, equal to 99.98% ($n=3$) in the 6.0 N HCl fraction.

² Seawater sample volumes greater than 240 ml could be readily processed by this method to improve signal intensity and the signal-to-blank ratio. The volumes utilized here reflect the 500 ml samples collected by the MITESS system and the measurement of additional elemental or isotopic systems from these bottles.

2.2. MC-ICP-MS configuration

Lead isotope analysis was completed on a Micro-mass IsoProbe ICP-MS at MIT, including the standard instrumental configuration under Class 100 conditions. General instrumental parameters are given in Table 1. The introduction system includes a Teflon microconcentric nebulizer (Microflow PFA-100, 100 $\mu\text{l min}^{-1}$, Elemental Scientific), a cyclonic spray chamber cooled to 4 °C (Jacketed Twister, Glass Expansion), and a Fassel quartz torch (Glass Expansion). Experiments with multiple introduction methods showed improved isotope ratio precision with the PFA nebulizer, peristaltic pumping, and small internal diameter pump tubing (0.19 mm ID, Ismatec). This improvement in precision might reflect the constant solution flux relative to natural draw conditions, which can be affected by variations in the argon mass flow controller. The water-cooled interface includes nickel sampling, skimmer, and collimator cones with an accelerating potential of -600 V (at 40% extraction). The accelerated ion beam is axially focused and thermalized within a 6-MHz, RF-only hexapole-collision cell, reducing the energy range of the incoming ions from 30 to approximately 1 V. The theoretical limit for ^{208}Pb thermalization by ^{40}Ar equals 0.1 V. A compromise is required, however, between transmission and the

Table 1
IsoProbe MC-ICP-MS instrumental conditions

Parameter	Set point	Unit
Nebulizer gas	0.905	l min^{-1}
Auxiliary gas	0.890	l min^{-1}
Cool gas	13.5	l min^{-1}
Forward power	1350	W
Reflected power	<3	W
Expansion Pirani	$3.00\text{e}-01$	mbar
Intermediate Pirani	$1.00\text{e}-02$	mbar
Analyzer Pirani	<0.01	mbar
Hexapole ion gauge	$3.20\text{e}-04$	mbar
Analyzer ion gauge	$1.10\text{e}-08$	mbar
Acquisition time	250	s
Uptake rate	100	$\mu\text{l min}^{-1}$
^{209}Bi sensitivity	$2.1\text{e}+06$	cps ppb^{-1}

The hexapole ion gauge pressure includes a collision cell argon gas flow rate of $1.500 \text{ ml min}^{-1}$, and the analyzer pressure has varied from 1.1×10^{-8} to 2.2×10^{-8} mbar over 7 months. The acquisition time reflects twenty-five 10-s integrations.

ion energy distribution, increasing the average ion energy to approximately 1 V (Turner et al., 2000). The thermalized ions are then focused by five electrostatic lenses (extraction, Y-focus, Y-slit, Z-focus, Z-slit) with a final acceleration potential of -6000 V. Following the lens stack, the ions are separated by a stigmatic-focusing, Cross geometry magnet reviewed by Turner et al. (2000). Finally, the separated ions are detected with a dynamic multiple collector array, consisting of seven Channeltron electron multipliers, eight Faraday collectors, and one axial Daly detector.

A quantitative estimate of the true analyte intensity (I_t) from the measured intensity (I_m) requires several established corrections (see Thirlwall, 2001), including mass spectral backgrounds associated with the Faraday cup offsets (I_{ms}), the solvent blank (I_s), the instrumental blank (I_i), the procedural blank (I_p)³, isobaric interferences (I_{iso}), and tailing from adjacent masses (± 3 amu, I_{tail}). This can be written as:

$$I_t = I_m - I_{ms} - I_s - I_i - I_p - I_{iso} - I_{tail} \quad (1)$$

The first three corrections (I_{ms} , I_s , and I_i) are determined by on-peak zero (OPZ) analysis for each measurement, continuously monitored to assess sample or standard memory effects. Prior to OPZ measurements, washout intervals of at least 6 min were used with 0.5 N HNO₃ and 0.5 N HCl, monitoring both signal intensity and the isotope ratios. Two procedural blanks were analyzed for every column series ($n=14$), and representative blanks range from 1.2 to 4.9 pg. The isotopic composition of the procedural blank could not be accurately determined by static Faraday collection given the low signal intensity (the calculated ²⁰⁶Pb/²⁰⁷Pb range was 0.832–1.033). No isobaric interference corrections are required for ²⁰⁶Pb, ²⁰⁷Pb, and ²⁰⁸Pb analyses, whereas ²⁰⁴Pb measurements require ²⁰⁴Hg correction via ²⁰²Hg. Finally, the tailing correction must include the abundance sensitivity (AS) for each peak (i) three⁴ mass

units above and below the analyte mass, determined by analysis of the monoisotopic ²⁰⁹Bi (Thirlwall, 2001). This is given simply as:

$$I_{tail} = \sum_{i=-3}^3 I_i \cdot AS_i \quad (2)$$

where I_i reflects the on-peak intensity ± 3 amu and AS_i denotes the corresponding abundance sensitivity. Static and scanning analyses of ²⁰⁹Bi were completed weekly or following any pressure shift. With an analyzer pressure of 1.1×10^{-8} mbar, the average abundance sensitivities relative to ²⁰⁹Bi are as follows: 2.5 ppm (-3 amu), 4.4 ppm (-2 amu), 13.6 ppm (-1 amu), 6.1 ppm ($+1$ amu), 5.9 ppm ($+2$ amu), and 3.1 ppm ($+3$ amu). These values are stable to ± 2 ppm (2σ) under the same vacuum conditions. Comparable results to Thirlwall (2001) were observed at -1 amu (mass 208; 23.4 ppm: MIT; 21.0 ppm: Royal Holloway) at similar analyzer pressures (2.2×10^{-8} mbar: MIT, 2.5×10^{-8} mbar: Royal Holloway). Systematic correction techniques thus presently exist to account for procedural, reagent, instrumental, and mass spectral contributions.

Finally, the small sample masses analyzed here preclude precise ²⁰⁶Pb/²⁰⁴Pb analysis. With moderate-volume North Atlantic seawater samples (0.160 kg, 38.1 pmol kg⁻¹ for 1999) and the parameters given in Table 1, the ion counting statistic for the ²⁰⁶Pb/²⁰⁴Pb ratio is 489 ppm (2σ). The limit does not include Faraday cup noise (~ 700 ppm 2σ at 1.5×10^{-12} A ²⁰⁸Pb) and uncertainties associated with the ²⁰⁴Hg correction. Low signal intensities limit accurate and precise ²⁰⁴Pb ratio analysis under these conditions; the focus of this study will be ²⁰⁷Pb/²⁰⁶Pb and ²⁰⁸Pb/²⁰⁶Pb determinations.

3. Results and discussion

Several MC-ICP-MS experiments are presented, including mass bias effects, isotope ratio precision, and matrix effects. These observations are not necessarily applicable to other instruments, isotopic systems, or interface configurations (e.g., cool plasma, shielded torch). These results provide, however, a

³ Defined here as the cumulative lead derived from the sample processing sequence, including sample handling, cleaning reagents, acids, bases, and the anion exchange column.

⁴ The mass range is determined by tailing of the high-abundance peaks. If ²⁰⁴Pb is to be accurately determined, a ± 4 amu range must be used to account for ²⁰⁸Pb tailing.

simple and consistent framework for lead isotope ratio analysis by the IsoProbe MC-ICP-MS.

3.1. Mass bias in MC-ICP-MS

Mass discrimination is a well-known phenomenon in ICP-MS systems, resulting from space charge repulsion and ion beam defocusing effects (see review by Niu and Houk, 1996). Space charge effects in ICP-MS generally result in preferential heavy ion transmission: following charge separation between the sampling and skimmer cones, increased positive ion density behind the skimmer repels lighter ions, whereas heavy ions remain axially focused (see Plate 1 in Montaser, 1998). Preferential light ion transmission can also result from space charge effects, dependent upon the ion optics and sample matrix. For example, Beauchemin et al. (1987) observed enhanced ^{59}Co , ^{63}Cu , and ^{64}Zn sensitivity relative to ^{114}Cd and ^{208}Pb in a 0.01 M Na solution (see their Fig. 2c). Elemental bias has also been demonstrated by simulation modeling, ion current observations, ion deposition experiments, and tandem quadrupole TOF observations (Gillson et al., 1988; Chen and Houk, 1996; Allen et al., 1997; Burgoyne et al., 1997). Comparable isotopic observations do not presently exist for MC-ICP-MS systems, requiring empirical corrections to quantify mass discrimination.⁵

Mass bias corrections for TIMS and MC-ICP-MS systems have been successfully developed by double- and triple-spiking methods (see Thirlwall, 2000, 2001 and references therein), quantifying mass discrimination and the true isotopic ratio by comparison of spiked and unspiked samples. An alternative technique for MC-ICP-MS lead isotope analysis is thallium normalization (Longerich et al., 1987). This method relies on concurrent analysis of a thallium isotopic standard, applying the calculated mass bias factor to the lead isotope ratios. Here the exponential empirical correction was assumed, and differences among these corrections will be addressed. For exponential bias, the true (t) $^{205}\text{Tl}/^{203}\text{Tl}$ ratio can be determined via the

measured ratio (m), the mass ratio (M_{205}/M_{203}), and an exponential bias factor (β):

$$\left(\frac{^{205}\text{Tl}}{^{203}\text{Tl}}\right)_t = \left(\frac{^{205}\text{Tl}}{^{203}\text{Tl}}\right)_m \left(\frac{M_{205}}{M_{203}}\right)^\beta \quad (3)$$

Applying the thallium bias factor (β_{Tl}) to lead, one can simultaneously correct for instrumental mass discrimination.

To test these assumptions, a stock 32 nM SRM-981 standard was repeatedly analyzed. Mass bias was induced by atypically large adjustments of the nebulizer gas flow rate and the extraction lens potential, motivated by the observations of Burgoyne et al. (1997, see their Fig. 4). The nebulizer flow rate and extraction potential represent two possible tuning parameters of the plasma interface, and these results are not necessarily applicable to other interface variables (torch position, torch power, argon flow rates, or cone positions). These two parameters, however, will directly change the sampling depths, ion optics, and mass bias of the ICP-MS interface. Established blank and background corrections were completed prior to each analysis, and the results are shown in Fig. 1. For optimized instrumental conditions (0.890–0.910 l Ar min^{-1} , 30–40% extraction), the mass bias factor is approximately $\beta = -1.2$ (0.7% amu^{-1}), corresponding to the expected preferential heavy ion transmission. Increased nebulizer flow rates result in reduced sampling depths, diminished solvent loading (via reduced solvent-to-gas ratios with constant peristaltic pumping), and a defocused ion beam. At approximately 0.925 l min^{-1} , significant light ion transmission was observed ($\beta = 0.864$). This effect is not strongly correlated to the ^{208}Pb signal intensity ($r = -0.72$), with approximately constant bias despite a 35% increase in ^{208}Pb intensity from 0.870 to 0.900 l min^{-1} . Second, the extraction potential was reduced, decreasing the ion beam intensity and increasing the mass bias factor ($r = -0.99$). Both results follow the expected relationship between space charge effects and mass bias: as ion beam intensities drop, greater light ion transmission occurs. The magnitude of this effect, including positive mass bias factors, was unexpected, and a complete explanation requires ion trajectory modeling under comparable conditions.

⁵ The empirical nature of these corrections is emphasized, based on the complexity of an accelerating, densely charged, high-temperature plasma through the ICP-MS interface.

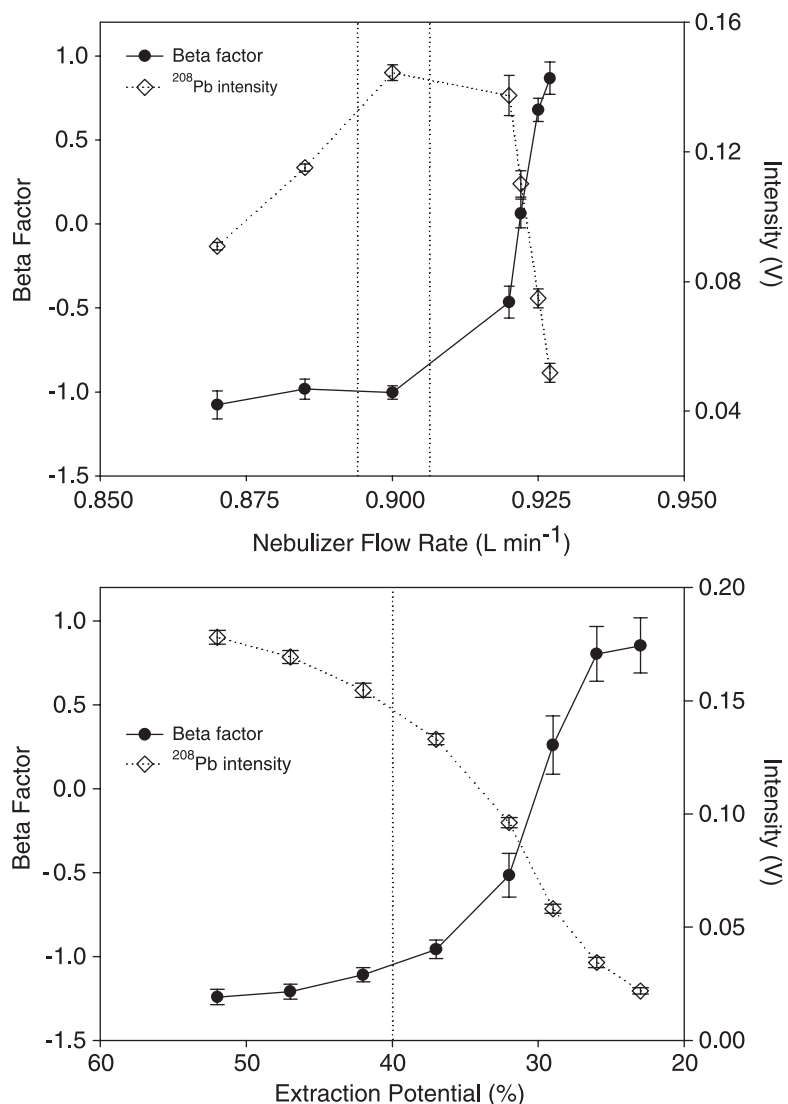


Fig. 1. IsoProbe mass bias experiments. The open diamonds reflect the ^{208}Pb intensity for each experiment, and the closed circles denote the exponential bias factor (β). The left abscissas correspond to the exponential mass bias factor, and the right abscissas reflect ^{208}Pb intensities. Nebulizer flow rate (l min^{-1}) and extraction potential (%) are given on the upper and lower panels, respectively. The dashed vertical lines correspond to typical adjustment values for the nebulizer flow rate ($0.895\text{--}0.905 \text{ l min}^{-1}$) and the extraction potential (fixed at 40%). Error bars are $\pm 2\sigma$ standard deviation of internal replicates ($n=25$).

3.2. Lead isotope ratio accuracy

The mass bias results were then utilized to test the empirical corrections, following the method of Russell et al. (1978). These artificial techniques are not equivalent to standard IsoProbe operating conditions; the large resulting β range, however, provides an im-

proved constraint for the model validation. As shown in Fig. 2, the measured $^{207}\text{Pb}/^{206}\text{Pb}$ and $^{205}\text{Tl}/^{203}\text{Tl}$ ratios were normalized via the assumed true isotope ratios from Thirlwall (2000) and Dunstan et al. (1980), respectively. As shown in Table 2, best agreement among SRM-981 $^{207}\text{Pb}/^{206}\text{Pb}$ and $^{208}\text{Pb}/^{206}\text{Pb}$ ratios is observed for the $^{207}\text{Pb}\text{--}^{204}\text{Pb}$ double-spike (Thirlwall,

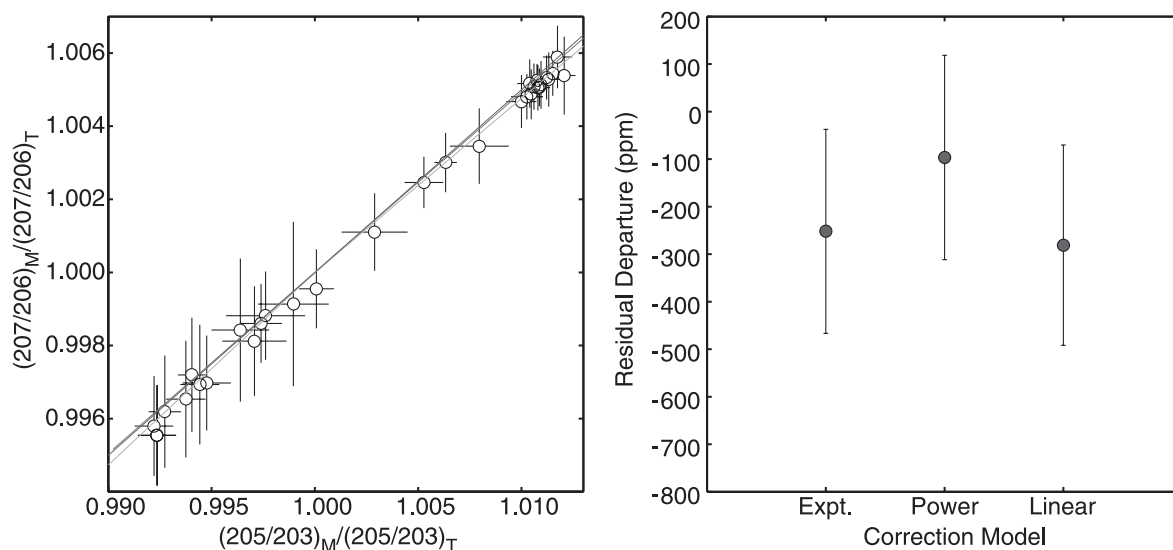


Fig. 2. Empirical mass bias models for MC-ICP-MS. The left panel shows the normalized lead and thallium ratios and the corresponding mass bias models. The solid lines reflect the linear and exponential models, and the dashed line reflects the power law model. Error bars are $\pm 2\sigma$ standard deviation of internal replicates ($n=25$). The right panel shows the mean and external 2σ standard deviation for the model residuals. Differences among models are not significant at the 95% confidence interval.

2000) and ^{207}Pb – ^{206}Pb – ^{204}Pb triple-spike (Galer and Abouchami, 1998) TIMS methods; the Thirlwall (2000) double-spike results were selected as the refer-

ence ratios for this study. The exponential ($R_t = R_m(M_2/M_1)^\beta$), power ($R_t = R_m(1 + \beta)^{M_2/M_1}$), and linear ($R_t = R_m[1 + \beta(M_2 - M_1)]$) corrections were then cal-

Table 2

SRM-981 compilation, TIMS and MC-ICP-MS

No.	$^{207}\text{Pb}/^{206}\text{Pb}$	2σ	$^{208}\text{Pb}/^{206}\text{Pb}$	2σ	n	Reference	Method
1	0.91469	0.00007	2.16770	0.00021	31	Thirlwall (2000)	^{207}Pb – ^{204}Pb double spike
2	0.91475	0.00004	2.16771	0.00010	60	Galer and Abouchami (1998)	^{207}Pb – ^{206}Pb – ^{204}Pb triple spike
3	0.91459	0.00013	2.16701	0.00043	11	Todt et al. (1996)	^{205}Pb – ^{202}Pb double spike
4	0.91468	0.00037	2.16733	0.00052	109	Woodhead et al. (1995)	^{207}Pb – ^{204}Pb double spike
5	0.91472	0.00053	2.16747	0.00144	10	Hamelin et al. (1985)	^{207}Pb – ^{204}Pb double spike
	0.91472	0.00007	2.16771	0.00050	2	Mean TIMS	(1) and (2)
6	0.91488	0.00008	2.16770	0.00024	36	Thirlwall (2000)	^{207}Pb – ^{204}Pb double spike
7	0.91470	0.00016	2.16686	0.00068	25	Thirlwall (2000)	Tl, exp corr, $^{205}\text{Tl}/^{203}\text{Tl}=2.38890$
8	0.91455	0.00007	2.16693	0.00020	8	Rehkämper and Mezger (2000)	Tl, exp corr, $^{205}\text{Tl}/^{203}\text{Tl}=2.38705$
9	0.91450	0.00005	2.16589	0.00014	32	Rehkämper and Halliday (1998)	Tl, exp corr, $^{205}\text{Tl}/^{203}\text{Tl}=2.38710$
10	0.91459	0.00005	2.16629	0.00014	32	Rehkämper and Halliday (1998)	Tl, exp corr, $^{205}\text{Tl}/^{203}\text{Tl}=2.38755$
11	0.91433	0.00003	2.16469	0.00086	8	Hirata (1996)	Tl, power corr
12	0.91462	0.00004	2.16636	0.00082	8	Hirata (1996)	Tl, power and β corr
	0.91460	0.00018	2.16639	0.00304	7	Mean MC-ICP-MS	(6) to (12)
	0.91474	0.00042	2.16701	0.00084	12	This study	Tl, exp corr
	0.91472	0.00016	2.16776	0.00052	12	This study	Tl, exp corr, renormalized to [1]

Studies 1–5 reflect TIMS double- or triple-spike techniques (Hamelin et al., 1985; Woodhead et al., 1995; Todt et al., 1996; Galer and Abouchami, 1998; Thirlwall, 2000), whereas the final seven studies utilize thallium normalization or double-spike techniques with MC-ICP-MS (Hirata, 1996; Rehkämper and Halliday, 1998; Rehkämper and Mezger, 2000; Thirlwall, 2000).

Note the agreement between Thirlwall (2000) and Galer and Abouchami (1998) for both the $^{207}\text{Pb}/^{206}\text{Pb}$ and $^{208}\text{Pb}/^{206}\text{Pb}$ ratios. The MC-ICP-MS results exhibit greater uncertainty with respect to $^{208}\text{Pb}/^{206}\text{Pb}$, and our results are within error of the TIMS observations.

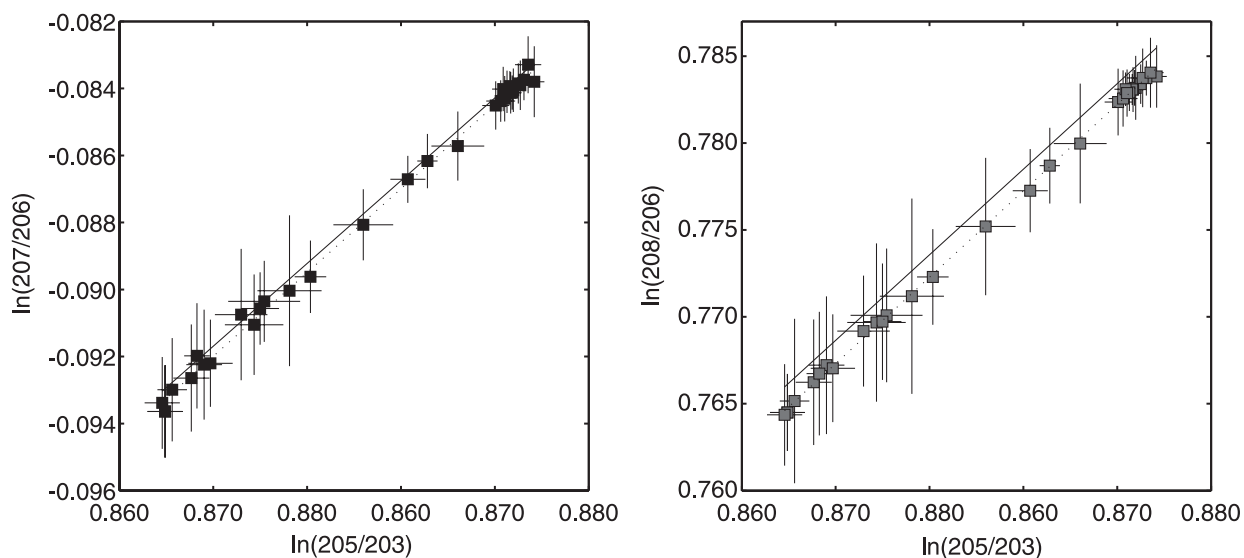


Fig. 3. Log transforms of $^{207}\text{Pb}/^{206}\text{Pb}$, $^{208}\text{Pb}/^{206}\text{Pb}$, and $^{205}\text{Tl}/^{203}\text{Tl}$. The solid line corresponds to the theoretical slope and intercept calculated from the assumed true isotopic ratios (see text), whereas the dotted lines reflect type-II linear regressions (York, 1966). The resulting slopes, intercepts, and uncertainties are given in Table 3, and the differences between the observed and theoretical slopes are not significant at the 95% confidence interval. Error bars are $\pm 2\sigma$ standard deviation of internal replicates ($n=25$).

culated for a given β range (-1 to 2). No difference is apparent between the linear and exponential models, whereas the power law better fits the $^{207}\text{Pb}/^{206}\text{Pb}$ extrema. For the $^{208}\text{Pb}/^{206}\text{Pb}$ ratio (not shown), the improved power law fit is not observed. The accuracy of the model residuals should not be overstated (here -289 to -101 ppm), as they assume ‘true’ isotopic ratios and equivalent bias factors for thallium and lead. The large standard deviations (220 ppm, 2σ) suggest these interface experiments represent a worst-case scenario, and the three models are comparable under these conditions.

A second consideration is the assumed equivalence of the mass bias factors, β_{Pb} and β_{Tl} . Hirata (1996) observed a linear dependence between mass discrimi-

nation and atomic mass (85–208 amu), and improved accuracy was observed with a $\beta_{\text{Pb}}/\beta_{\text{Tl}}$ correction. The Hirata (1996) correction was determined by measuring the slope of the mass bias trend versus atomic mass from ^{85}Rb to ^{208}Pb , then calculating the $\beta_{\text{Pb}}/\beta_{\text{Tl}}$ ratio from the slope and intermediate masses of Tl (204) and Pb (206.5). To test this method, the $\beta_{\text{Pb}}/\beta_{\text{Tl}}$ ratio was calculated according to Maréchal et al. (1999), shown in Fig. 3 and Table 3. Differences among the four beta ratios are not statistically significant at the 95% confidence interval, and all ratios are within error of unity. In contrast to Hirata (1996), the $\beta_{\text{Pb}}/\beta_{\text{Tl}}$ correction offers slight improvement over standard thallium normalization (Table 4), whereas correction of the ‘true’ $^{205}\text{Tl}/^{203}\text{Tl}$ ratio greatly improves isotope ratio accura-

Table 3
SRM-981 mass bias experiment

Ratio	(Slope) _T	(Slope) _M	($\beta_{\text{Pb}}/\beta_{\text{Tl}}$) _M	(Intercept) _T	(Intercept) _M	($\beta_{\text{Pb}}/\beta_{\text{Tl}}$) _b
208/206	0.98555	0.99191	1.00645	−0.08384	−0.09063	1.00792
2σ	†	0.00908	0.00921	0.0002	0.00849	0.00927
207/206	0.49413	0.49517	1.0021	−0.5191	−0.52028	1.00273
2σ	†	0.00995	0.02014	0.00012	0.0093	0.02163

The theoretical (T) slope and intercept for the regression are given, utilizing the isotopic ratios of Dunstan et al. (1980) and Thirlwall (2000) for the intercept. The measured (M) slopes and intercepts are taken from Fig. 3. No uncertainty in the atomic masses is assumed (†), and the 2σ standard deviation for columns 4, 5, and 7 are determined by error propagation.

Table 4
SRM-981 accuracy experiment

Isotope ratio	R_1	Δ_1	R_2	Δ_2	R_3	Δ_3
$^{208}\text{Pb}/^{206}\text{Pb}$	2.16507	-1213	2.16512	-1189	2.16774	17
$^{207}\text{Pb}/^{206}\text{Pb}$	0.91446	-256	0.91446	-252	0.91469	4

Here R_x reflects three correction experiments, and Δ corresponds to the respective departures (in ppm) from Thirlwall (2000). Experiment 1 represents thallium normalization, experiment 2 reflects the $\beta_{\text{Pb}}/\beta_{\text{Tl}}$ correction of Hirata (1996), and experiment 3 corresponds to the true $^{205}\text{Tl}/^{203}\text{Tl}$ correction of Rehkämper and Halliday (1998). The anomalously large Δ values reflect the instrumental conditions shown in Fig. 1.

cy (see Rehkämper and Halliday, 1998). We suggest this difference results from secondary bias effects discussed by White et al. (2000), including Faraday cup efficiencies, amplifier gains, and ion optics (e.g., misalignment of the image focal plane with respect to the detector array). A simple rationale for this effect is given in Appendix A. The $\beta_{\text{Pb}}/\beta_{\text{Tl}}$ correction cannot be discounted for other instruments or configurations, given its successful application by Hirata (1996). For these experimental conditions, however, variations in the $\beta_{\text{Pb}}/\beta_{\text{Tl}}$ ratio alone cannot completely explain instrumental mass bias.

Secondary mass bias effects can be directly addressed by the MC-ICP-MS double-spiking technique of Thirlwall (2000), accounting for the cumulative mass bias of a sample and known isotopic spike. An alternative solution is external normalization to SRM-981 following Tl normalization (modified from Belshaw et al., 1998). This method requires an assumed ‘true’ isotopic ratio typically determined by TIMS double- or triple-spiking techniques (see references in Table 2). As the accepted SRM-981 isotopic ratios are better constrained, the resulting data sets must be accordingly renormalized. These corrections are also significant relative to the analytical precision (see below), ranging from -304 to 220 ppm ($n=12$) over 6 months. However, the secondary correction factors are stable on weekly to monthly time scales, are precisely determined by daily replicate analyses, and provide a simple solution to secondary mass bias effects.

3.3. Lead isotope ratio precision

Instrumental mass bias directly affects isotope ratio precision, and three separate experiments were com-

pleted for its assessment. First, short-term stability over 14 days was tested, including multiple glassware, nebulizer, interface, and hexapole configurations. These experiments were consistently completed after 90 min of torch ignition, providing an estimate of worst-case, hourly departures. Following thallium normalization, the first block of four (as thirty 10-s integrations) was used to determine secondary normalization factors for the remaining three blocks (assuming true ratios from Thirlwall, 2000). The results are shown in Fig. 4, and the 2σ relative standard deviations for the $^{207}\text{Pb}/^{206}\text{Pb}$ and $^{208}\text{Pb}/^{206}\text{Pb}$ ratios are 75 and 110 ppm, respectively. Second, SRM-981 was analyzed 22 times over 16 h to assess daily isotope ratio stability, calculating the secondary normalization factors with bracketing standards. No instrument parameters were altered during this experiment, and the resulting deviations are 142 ($^{207}\text{Pb}/^{206}\text{Pb}$) and 172 ($^{208}\text{Pb}/^{206}\text{Pb}$) ppm. Finally, a stock SRM-981 standard was analyzed every three samples for 12 analytical sessions. The resulting daily vector of n SRM-981 analyses was divided into alternating ‘standards’ [1:2:n] and ‘samples’ [2:2:n-1], determining the secondary normalization factors from the daily ‘standard’ average. No significant trends in the isotopic ratios were observed for the 12 sessions, and the resulting 2σ deviations are 177 ($^{207}\text{Pb}/^{206}\text{Pb}$) and 240 ($^{208}\text{Pb}/^{206}\text{Pb}$) ppm. This final estimate is the most realistic, because it includes multiple analytical sessions (12–16 h), variable sample and standard matrices, and possible memory effects. The respective counting statistics for the third experiment are 93 and 77 ppm; approximately one third to one half of the uncertainty can be ascribed to the limited signal intensity.

The external precision should be considered within the context of this application. Previous lead isotope analysis from western North Atlantic surface corals ranged from 1.184 to 1.215 with respect to $^{207}\text{Pb}/^{206}\text{Pb}$, or 25,844 ppm (Shen and Boyle, 1987). The isotopic range in the modern (1987–1989) North Atlantic mixed layer is comparable (1.166–1.197, Véron et al., 1993; Hamelin et al., 1997; Weiss et al., 2000). The highest external precision estimate given above (240 ppm) corresponds to a signal-to-noise ratio of 108. The MC-ICP-MS method shown here is thus adequate for both surface corals and seawater, quantitatively resolving modern isotopic variability.

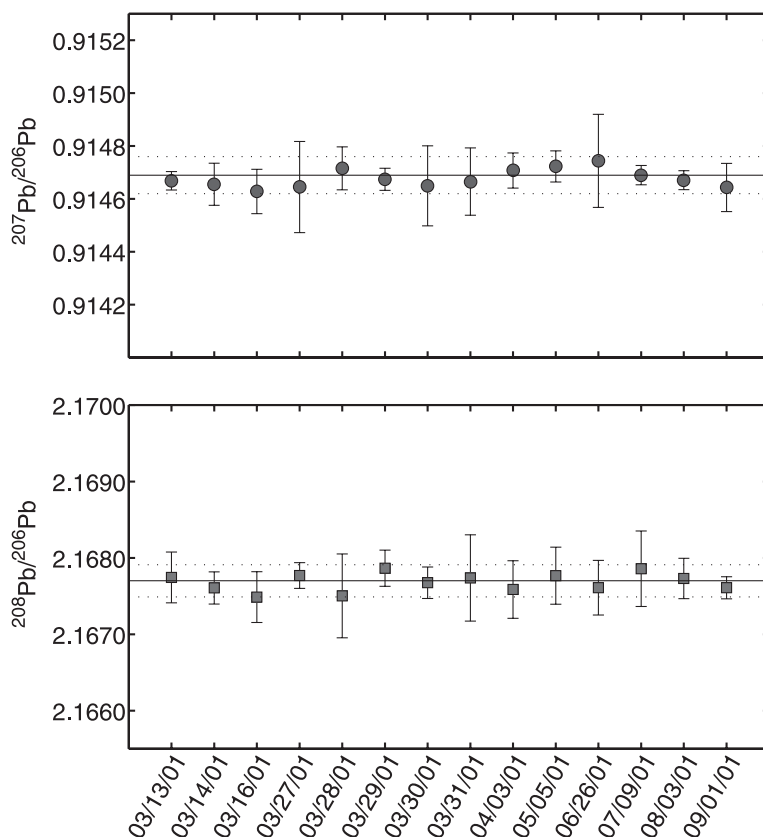


Fig. 4. SRM-981 external precision experiments. The upper panel represents the mean and external 2σ standard deviation for the $^{207}\text{Pb}/^{206}\text{Pb}$ ratio (75 ppm), and the lower panel reflects the $^{208}\text{Pb}/^{206}\text{Pb}$ ratio (110 ppm). The solid and dashed lines represent the mean and 2σ deviation of the Thirlwall (2000) TIMS double-spike analysis.

3.4. Matrix effects in MC-ICP-MS

Sample matrix effects represent an important consideration for MC-ICP-MS. Elevated concomitants generally increase space charge effects and heavy ion transmission in ICP-MS (see above), and the observed magnitude depends upon the analyte–concomitant mass difference, the concomitant concentration, and the nebulizer flow rate (see review by Horlick and Montaser, 1998). For this study, residual Ca^{2+} following anion exchange chromatography and column organics might affect isotope ratio precision and accuracy. To evaluate this effect, four gravimetric calcium standards (0.260–257 μM) were spiked with SRM-981 and thallium, measuring each isotopic standard four times. The matrix standards were deliberately measured in order of increasing calcium

concentration to simulate progressive salt deposition on the cone and skimmer. Instrumental parameters (e.g., nebulizer flow rate and torch position) were not adjusted throughout the analytical session. Calcium-free SRM-981 was analyzed before and after the experiment, and the results are shown in Fig. 5. Significant departures were observed for both isotopic ratios, with the 0.260 μM calcium standard exhibiting a -44 ppm departure from Thirlwall (2000). Higher calcium concentrations yielded greater offsets and diminished external precision, reaching -280 ppm for 257 μM [Ca]. During this experiment, the associated signal intensity was reduced by only 6%: the ^{208}Pb intensity ranged from 0.170 ± 0.002 to 0.160 ± 0.003 V for the initial and final calcium-free SRM-981 analyses, respectively. Significant mass bias shifts can thus occur with minor intensity variations.

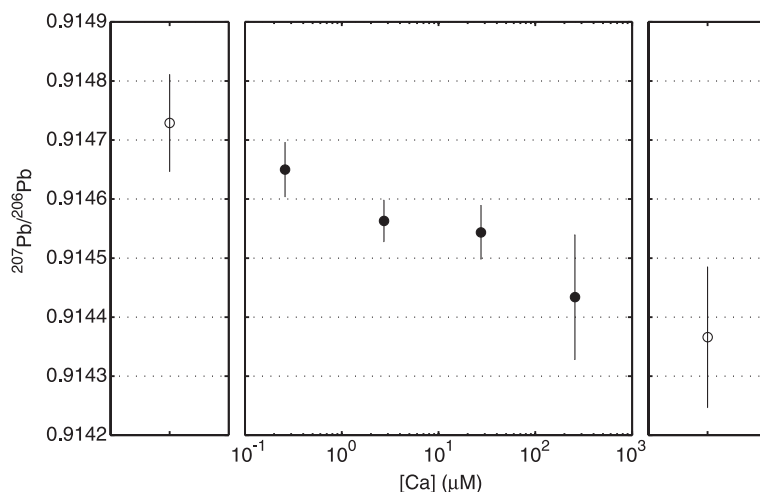


Fig. 5. IsoProbe calcium matrix experiments, SRM-981. The open circles represent calcium-free SRM-981 standards analyzed before and after the experiment. The closed circles reflect lead-free calcium standards (0.26–257 μM) spiked with SRM-981 and thallium. Each result includes the mean and external 2σ standard deviation of four analyses, and note the elevated light ion transmission with increasing calcium concentrations.

These results cannot be adequately explained by space charge effects, supported by three observations. First, the trend is in the opposite direction from the previous experiments, with increased concomitant calcium concentrations favoring light ion transmission. Second, the final calcium-free SRM-981 departure is -354 ppm, well outside the initial SRM-981 measurement error and in agreement with the previous matrix standard. Third, no mass bias effects have been observed for other isotopic systems, including 100 ppm Na and Al additions to U500 (Z. Palacz, personal communication). These matrix effects, however, are consistent with Fig. 1 and ion beam defocusing, governed in this case by salt deposition on the micro-flow nebulizer, sampling cone, and skimmer. Visible calcium deposition was observed after the experiments, resulting from repeated analysis of high-[Ca] solutions over a four hour period. As the ion flux is reduced through a smaller sampling orifice, the space charge effect might diminish due to lower ion densities, favoring the lighter ion. This result will not be observed, however, if the concomitant does not accumulate on the interface. Thus matrix effects are significant for precise isotope ratio analysis; external normalization with matrix-matched standards, however, offers one possible solution. For seawater and coral analysis, elimination of the major cations by anion

exchange chromatography and consistent matrix matching were adopted.

3.5. Method assessment and application

To assess this analytical technique, the SRM-981 accuracy and precision were compared to previous TIMS and MC-ICP-MS determinations. As a reference point, the double- and triple-spiking TIMS methods were first considered, and best agreement between the $^{207}\text{Pb}/^{206}\text{Pb}$ and $^{208}\text{Pb}/^{206}\text{Pb}$ ratios was observed for two studies (Galer and Abouchami, 1998; Thirlwall, 2000). The mean and 2σ standard deviation of the MC-ICP-MS analyses shown here agree with the TIMS result, although the overall external precision is reduced given secondary mass bias effects (see above). The results of this study are comparable to previous MC-ICP-MS SRM-981 measurements, with improved long-term external precision using secondary normalization. However, the signal intensities employed for this study (1.5×10^{-12} A) are at least one order of magnitude lower than previous observations, and reported ^{208}Pb intensities are typically greater than 3×10^{-11} A. Favorable $^{207}\text{Pb}/^{206}\text{Pb}$ and $^{208}\text{Pb}/^{206}\text{Pb}$ external precision is observed at considerably reduced signal intensities.

A brief case study of western North Atlantic surface corals and eastern North Atlantic seawater is provided to evaluate the proposed method. Additional detailed discussion of these North Atlantic results will be presented elsewhere. Surface coral cores (*Diploria strigosa* and *Diploria labyrinthiformis*) were collected from North Rock, Bermuda (32°29'N, 64°48'W) in 1983 by E. Druffel and co-workers. This site was selected based on its proximity to the North Atlantic subtropical gyre and no observed local anthropogenic lead influxes (Shen and Boyle, 1988b). The $^{206}\text{Pb}/^{207}\text{Pb}$ and $^{208}\text{Pb}/^{207}\text{Pb}$ results from 1886 to 2000 are shown in Fig. 6. These results include a seawater time series from the nearby Station S, Bermuda (32°10'N, 64°30'W), and the elemental time series data are provided in Wu and Boyle (1997a). The reconstructed isotopic variability agrees with the previous low-resolution surface coral isotopic record of Shen and Boyle (1988b), including

decreasing $^{206}\text{Pb}/^{207}\text{Pb}$ from 1886 to 1922, diminished $^{206}\text{Pb}/^{207}\text{Pb}$ variability from 1922 to 1968, and $^{206}\text{Pb}/^{207}\text{Pb}$ and $^{208}\text{Pb}/^{207}\text{Pb}$ maxima from 1968 to 1990. Most importantly, a $^{206}\text{Pb}/^{207}\text{Pb}$ difference of 250 ppm is observed between 1981 coral and 1982 seawater samples, supporting their separate processing methods, lead concentrations, and sample matrices. The seawater time series results are also consistent with previous thermal ionization results from the western North Atlantic (Véron et al., 1994; Hamelin et al., 1997). Therefore, the reconstructed North Atlantic $^{206}\text{Pb}/^{207}\text{Pb}$ and $^{208}\text{Pb}/^{207}\text{Pb}$ variability agrees with previous proxy records and seawater observations from multiple laboratories, best supporting the MC-ICP-MS technique.

Can the surface coral record be corroborated by historical anthropogenic lead variability? The multi-decadal $^{206}\text{Pb}/^{207}\text{Pb}$ and $^{208}\text{Pb}/^{207}\text{Pb}$ reduction from 1886 is consistent with increased combustion of

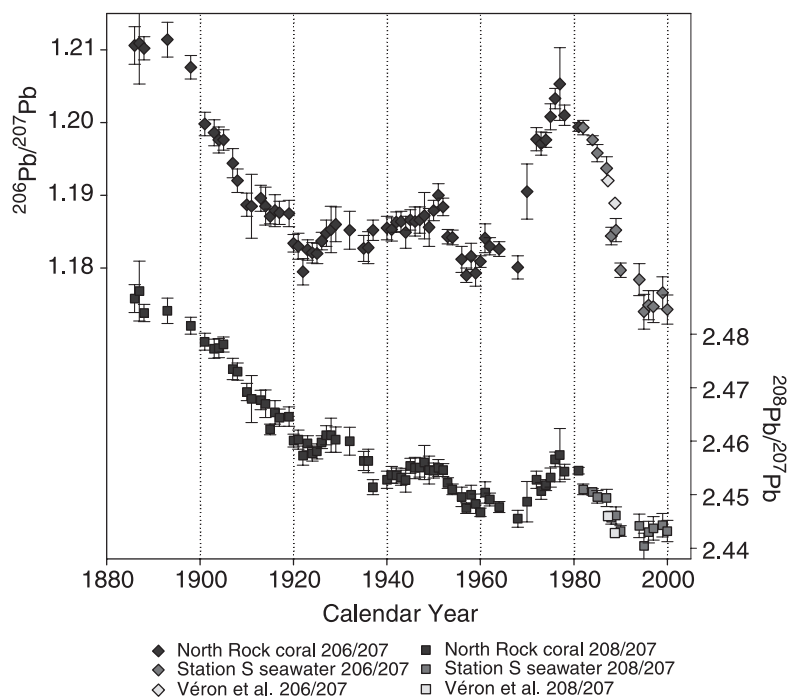


Fig. 6. Western North Atlantic surface coral proxy record and seawater time series, analyzed by MC-ICP-MS. Upper panel: Reconstructed $^{206}\text{Pb}/^{207}\text{Pb}$ ratio for Bermuda surface corals (closed circles) and western North Atlantic seawater (closed diamonds, Station S). The open squares reflect the TIMS seawater lead isotope analyses of Véron et al. (1994, sampled March 1987) and Hamelin et al. (1997, sampled August 1988). Lower panel: Same as above for $^{208}\text{Pb}/^{207}\text{Pb}$. Note the agreement among adjacent samples within the record and the isotopic range observed. Error bars are $\pm 2\sigma$.

North American coal (Chow and Earl, 1972), smelting of low $^{206}\text{Pb}/^{207}\text{Pb}$ – $^{208}\text{Pb}/^{207}\text{Pb}$ lead ores within North America, and other lead emissions throughout the Industrial Revolution (see review by Nriagu and Pacyna, 1988). Source apportionment during this period is difficult, however, given the similar $^{206}\text{Pb}/^{207}\text{Pb}$ – $^{208}\text{Pb}/^{207}\text{Pb}$ composition of the primary US lead ores and North American coals (e.g., Chow et al., 1975). Elevated $^{206}\text{Pb}/^{207}\text{Pb}$ and $^{208}\text{Pb}/^{207}\text{Pb}$ ratios from 1968 to 1990 is supported by a similar isotopic transition observed in San Diego aerosols (Chow et al., 1975), High Sierra lake sediments (Shirahata et al., 1980), and Chesapeake Bay sediments (Marcantonio et al., 2002). The increased $^{206}\text{Pb}/^{207}\text{Pb}$ and $^{208}\text{Pb}/^{207}\text{Pb}$ ratios can be linked to increased lead ore production from the southeast Missouri district: this region accounted for 40% of total US lead ore production in 1966, increasing to 93% in 1982 (United States Bureau of Mines, 1983). Given the elevated $^{206}\text{Pb}/^{207}\text{Pb}$ and $^{208}\text{Pb}/^{207}\text{Pb}$ signature of southeast Missouri ores (1.303 for $^{206}\text{Pb}/^{207}\text{Pb}$, Brown, 1967) and predominant US leaded gasoline consumption (80% with respect to North America and Europe, Wu and Boyle, 1997a), a corresponding North Atlantic isotopic shift is possible. As the subsequent $^{206}\text{Pb}/^{207}\text{Pb}$ reduction from 1982 to 2000 was not observed in recent Chesapeake Bay sediments (Marcantonio et al., 2002), one possible explanation is increased low- $^{206}\text{Pb}/^{207}\text{Pb}$ and $^{208}\text{Pb}/^{207}\text{Pb}$ European lead fluxes to the North Atlantic, consistent with higher relative European leaded gasoline consumption from 1982 (41%) to 1990 (74%, Wu and Boyle, 1997a). Therefore, the Bermuda coral record is consistent with historical patterns of anthropogenic lead fluxes to the North Atlantic and other proxy records.

The historical isotopic variability must have a corresponding seawater signature given the multi-decadal residence time of deep water lead estimated from ^{226}Ra – ^{210}Pb disequilibria. For example, Bacon et al. (1976) estimated integrated lead residence times of 20–93 years for six equatorial Atlantic stations (451–5003 m). To constrain the anthropogenic isotopic signature, seawater samples were collected from the eastern North Atlantic in 1999 (31°0'N, 31°0'W, R/V Endeavor-328), and the $^{206}\text{Pb}/^{207}\text{Pb}$ and [Pb] water column profiles are shown in Fig. 7. Elemental and isotopic analyses were completed on

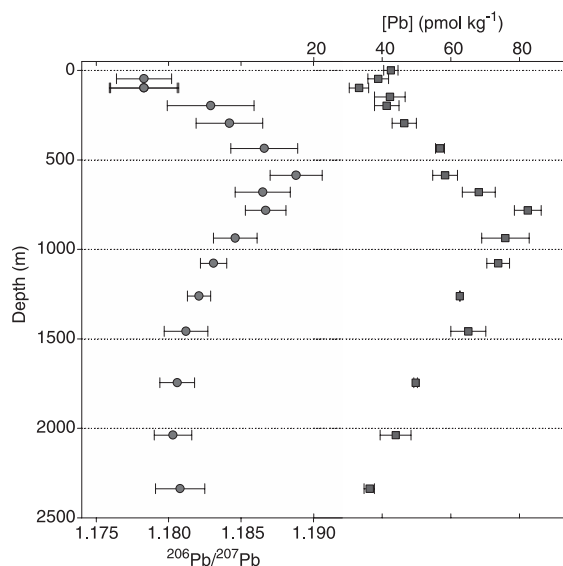


Fig. 7. Eastern North Atlantic stable lead isotope (MC-ICP-MS) and lead concentration profiles (ID-ICP-MS): Endeavor-328, Station 7 (31°0'N, 31°0'W). The left panel reflects the $^{206}\text{Pb}/^{207}\text{Pb}$ ratio, and the right panel denotes total lead concentrations. Note the observed upper thermocline maximum in $^{206}\text{Pb}/^{207}\text{Pb}$ and the agreement among mixed layer and deep water isotopic ratios. The depth difference of the elemental and isotopic maxima results from a 10-year phase lag between the elemental (1947–1990, not shown) and isotopic (1968–1990) North Atlantic lead transients. Error bars are $\pm 2\sigma$.

aliquots taken from the same sample bottles. First, the $^{206}\text{Pb}/^{207}\text{Pb}$ composition of eastern North Atlantic deep water (ca. 1.18) is significantly less than pre-industrial $^{206}\text{Pb}/^{207}\text{Pb}$ estimated from the coral record (1.2106 ± 0.0026 , see Fig. 6), implying addition of recent anthropogenic lead. Second, a $^{206}\text{Pb}/^{207}\text{Pb}$ maximum is observed at 586 m, resulting from the recent $^{206}\text{Pb}/^{207}\text{Pb}$ reduction and its delayed penetration to older water masses. The formation of this isotopic maximum is best shown by the western North Atlantic upper ocean $^{206}\text{Pb}/^{207}\text{Pb}$ time series (Fig. 8), including five profiles from 1984 to 1998. Note the shallower penetration depth of the $^{206}\text{Pb}/^{207}\text{Pb}$ maximum relative to the [Pb] profile, a possible consequence of the 10-year lag between the isotopic (1968–1990) and elemental (1947–1990, not shown) anthropogenic lead maxima and the shorter duration of the isotopic transient (22 versus 43 years). Thus the eastern North Atlantic seawater observations are consistent with the recon-

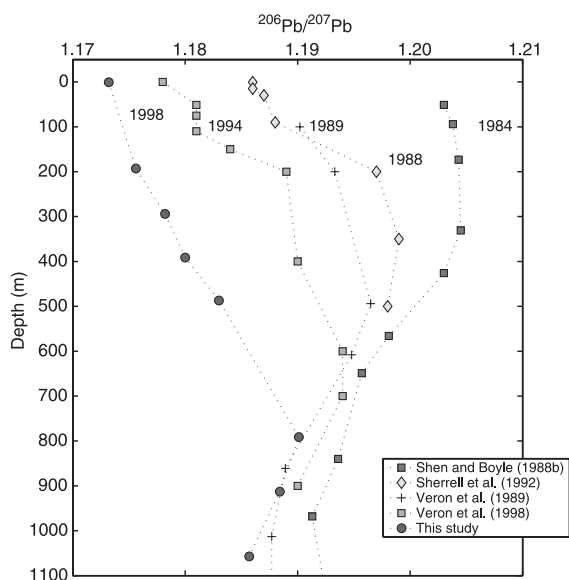


Fig. 8. Western North Atlantic thermocline $^{206}\text{Pb}/^{207}\text{Pb}$ evolution: 1984–1998. The profile data are from Shen and Boyle (1988b), sampled in 1984 at Station S, $32^{\circ}2'N$, $64^{\circ}30'W$), Sherrell et al. (1992, sampled in 1988 near Station S, $32^{\circ}0'N$, $64^{\circ}10'W$), Véron et al. (1993, sampled in 1989 at BATS, $31^{\circ}5'N$, $64^{\circ}1'W$), and this study (sampled in 1998 at $33^{\circ}42'N$, $57^{\circ}40'W$). Differences among site locations should be considered when interpreting these profiles. Note the consistent $^{206}\text{Pb}/^{207}\text{Pb}$ thermocline reduction and the isotopic maximum (ca. 800 m) in the 1998 profile.

structured isotopic variability and the western North Atlantic lead isotope profiles.

4. Conclusions

This analytical method represents a promising technique for lead isotope analysis. With signal intensities less than 1.5×10^{-12} A, external precision for the $^{207}\text{Pb}/^{206}\text{Pb}$ and $^{208}\text{Pb}/^{206}\text{Pb}$ ratios are consistently less than 250 ppm, ranging from 75 to 177 ppm for $^{207}\text{Pb}/^{206}\text{Pb}$ (2σ). Utilizing both thallium normalization and external correction to SRM-981, isotope ratio accuracy better than 250 ppm is possible, and the correction factors are stable on weekly to monthly time scales. For a typical analytical session (12–16 h), 30 samples and 12 standards can be analyzed. The MC-ICP-MS method provides a useful, rapid, and consistent method for $^{207}\text{Pb}/^{206}\text{Pb}$ and $^{208}\text{Pb}/^{206}\text{Pb}$ analysis of seawater and marine carbonates.

Acknowledgements

The suggestions and comments of Zenon Palacz and Simon Meffan-Main, Micromass UK, are gratefully acknowledged. Constructive reviews by Martin Frank and Jan Kosler also improved the quality of this manuscript. This work was supported by National Science Foundation grant OCE-0002273 to EAB. MKR is the recipient of a National Science Foundation Graduate Research Fellowship. [PD]

Appendix A

Mass bias in MC-ICP-MS has multiple potential sources, including the plasma interface, the ion optics, and the detector array. Here one rationale is presented for secondary bias effects, assuming the exponential mass bias law. This argument demonstrates the relative importance of the slope and intercept terms shown in Fig. 9. In the simplest case, variations in ion detection (e.g., collector efficiencies, amplifier

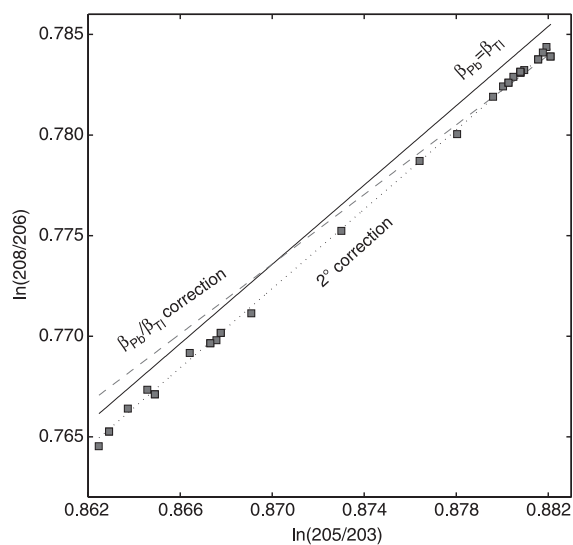


Fig. 9. Secondary bias correction for MC-ICP-MS, following Fig. 3. The solid line corresponds to the simplest case, where $\beta_{\text{Tl}} = \beta_{\text{Pb}}$, the dashed line includes a $\beta_{\text{Pb}}/\beta_{\text{Tl}}$ correction following Hirata (1996), and the dotted line reflects a secondary bias correction. Error bars are given in Fig. 3 and omitted for clarity.

gains, or ion optics) introduce a secondary bias factor into Eq. (3):

$$\left(\frac{^{205}\text{Tl}}{^{203}\text{Tl}}\right)_t = \left(\frac{^{205}\text{Tl}}{^{203}\text{Tl}}\right)_m \left(\frac{M_{205}}{M_{203}}\right)^\beta \alpha_1 \quad (4)$$

where α_1 corresponds to an arbitrary offset between two masses, and each isotope pair includes a separate gain factor. Collector efficiencies and amplifier gains are generally corrected by repeated analysis of multiple isotopic standards and constant current gain calibrations, respectively. However, improper focusing of the optical plane (K. Collerson, personal communication) and additional artifacts might introduce a secondary bias. For brevity, the atomic mass term for $^{205}\text{Tl}/^{203}\text{Tl}$ and $^{208}\text{Pb}/^{206}\text{Pb}$ (a constant) is assigned a new variable, τ :

$$\tau = \ln\left(\frac{M_{205}}{M_{203}}\right) / \ln\left(\frac{M_{208}}{M_{206}}\right) \quad (5)$$

Rewriting the Maréchal et al. (1999) derivation with the secondary bias factors for $^{205}\text{Tl}/^{203}\text{Tl}$ (α_1) and $^{208}\text{Pb}/^{206}\text{Pb}$ (α_2), one obtains:

$$\ln\left(\frac{^{208}\text{Pb}}{^{206}\text{Pb}}\right) = \left[\frac{1}{\tau} \frac{\beta_{\text{Pb}}}{\beta_{\text{Tl}}} \left(\frac{^{205}\text{Tl}}{^{203}\text{Tl}}\right)_m \right] + \left[\ln\left(\frac{^{208}\text{Pb}}{^{206}\text{Pb}}\right) - \ln(\alpha_2) \right]_t - \left[\frac{1}{\tau} \frac{\beta_{\text{Pb}}}{\beta_{\text{Tl}}} \ln\left(\frac{^{205}\text{Tl}}{^{203}\text{Tl}}\right) - \ln(\alpha_1) \right] \quad (6)$$

where α_1 and α_2 reflect the $^{205}\text{Tl}/^{203}\text{Tl}$ and $^{208}\text{Pb}/^{206}\text{Pb}$ secondary factors, respectively. As shown by Maréchal et al. (1999), this equation describes a line in the $\ln(^{205}\text{Tl}/^{203}\text{Tl}) - \ln(^{208}\text{Pb}/^{206}\text{Pb})$ domain, with the two arguments on the right-hand side corresponding to the slope and intercept terms, respectively. The primary result of Eq. (6) is the secondary factors are present only in the intercept term, graphically shown in Fig. 9. If one assumes $\beta_{\text{Pb}} = \beta_{\text{Tl}}$ for the secondary correction (Eq. 6), the slopes of the $\beta_{\text{Pb}} = \beta_{\text{Tl}}$ and secondary correction lines are equal by definition ($m = 1/\tau = 0.9855$) and within the 95% confidence interval of the observations ($m = 0.9919 \pm 0.0090$), providing additional evidence for the secondary bias. This difference provides a simple rationale for isotope ratio offsets observed in previous studies and the

$^{205}\text{Tl}/^{203}\text{Tl}$ optimization technique of Rehkämper and Halliday (1998). Secondary mass bias might also explain some of the 400 ppm amu^{-1} error observed by Thirlwall (2002) between ^{207}Pb – ^{204}Pb double-spiked and Tl-normalized SRM-981 analyses. Multiple independent correction techniques can account for this secondary bias effect, including double-spiking techniques, $^{205}\text{Tl}/^{203}\text{Tl}$ optimization, and secondary SRM-981 normalization.

References

- Alleman, L.Y., Véron, A.J., Church, T.M., Flegal, A.R., Hamelin, B., 1999. Invasion of the abyssal North Atlantic by modern anthropogenic lead. *Geophys. Res. Lett.* 26 (10), 1477–1480.
- Allen, L.A., Leach, J.L., Houk, R.S., 1997. Spatial location of the space charge effect in individual ion clouds using monodisperse dried microparticulate injection with a twin quadrupole inductively coupled plasma mass spectrometer. *Anal. Chem.* 69, 2384–2391.
- Bacon, M.P., Spencer, D.W., Brewer, P.G., 1976. $^{210}\text{Pb}/^{226}\text{Ra}$ and $^{210}\text{Pb}/^{210}\text{Po}$ disequilibrium in seawater and suspended particulate matter. *Earth Planet. Sci. Lett.* 32, 277–296.
- Beauchemin, D., McLaren, J.W., Berman, S.S., 1987. Study of the effects of concomitant elements in inductively coupled plasma mass spectrometry. *Spectrochim. Acta* 42B (3), 467–490.
- Belshaw, N.S., Freedman, P.A., O’Nions, R.K., Frank, M., Guo, Y., 1998. A new variable dispersion double-focusing plasma mass spectrometer with performance illustrated for Pb isotopes. *Int. J. Mass Spectrom.* 181, 51–58.
- Bollhöfer, A., Rosman, K.J.R., 2001. Isotopic source signatures for atmospheric lead: the Northern Hemisphere. *Geochim. Cosmochim. Acta* 65 (11), 1727–1740.
- Brown, J.S., 1967. Isotopic zoning of lead and sulfur in southeast Missouri. Genesis of stratiform lead–zinc–fluorite deposits (Mississippi Valley type deposits). *Econ. Geol.*, New York, 410–425.
- Burgoyne, T.W., Hieftje, G.M., Hites, R.A., 1997. Space charge evaluation in a plasma-source mass spectrograph. *Anal. Chem.* 69, 485–489.
- Chen, X.S., Houk, R.S., 1996. Spatially resolved measurements of ion density behind the skimmer of an inductively coupled plasma mass spectrometer. *Spectrochim. Acta* 51B (1), 41–54.
- Chow, T.J., Earl, J.L., 1970. Lead aerosols in the atmosphere: increasing concentrations. *Science* 169 (3945), 577–580.
- Chow, T.J., Earl, J.L., 1972. Lead isotopes in North American coals. *Science* 176 (4034), 510–511.
- Chow, T.J., Johnstone, M.S., 1965. Lead isotopes in gasoline and aerosols of Los Angeles Basin, California. *Science* 147, 502–503.
- Chow, T.J., Bruland, K.W., Bertine, K., Soutar, A., Koide, M., Goldberg, E.D., 1973. Lead pollution: records in southern California coastal sediments. *Science* 181, 551–552.
- Chow, T.J., Snyder, C.B., Earl, J.L., 1975. Isotope ratios of lead as

- pollutant source indicators. Proceedings of the International Atomic Energy Agency, Vienna, vol. 191 (4), pp. 95–108.
- Church, T.M., Véron, A.J., Patterson, C.C., Settle, D., Erel, Y., Maring, H.R., Flegal, A.R., 1990. Trace elements in the North Atlantic troposphere: shipboard results of precipitation and aerosols. *Glob. Biogeochem. Cycles* 4 (4), 431–443.
- Dickey, T., Frye, D., Jannasch, H., Boyle, E., Manov, D., Sigurdson, D., McNeil, J., Stramska, M., Michaels, A., Nelson, N., Siegel, D., Chang, G., Wu, J., Knap, A., 1998. Initial results from the Bermuda Testbed Mooring program. *Deep-Sea Res. I* (45), 771–794.
- Dunstan, L.P., Gramlich, J.W., Barnes, I.L., Purdy, W.C., 1980. Absolute isotopic abundance and the atomic weight of a reference sample of thallium. *J. Res. Natl. Bur. Stand.* 85, 1–10.
- Flegal, A.R., Itoh, K., Patterson, C.C., Wong, C.S., 1986. Vertical profile of lead isotopic compositions in the north-east Pacific. *Nature* 321, 689–690.
- Galer, S.J.G., Abouchami, W., 1998. Practical application of lead triple spiking for correction of instrumental mass discrimination. *Mineral. Mag.* 62A, 491–492.
- Gillson, G.R., Douglas, D.J., Fulford, J.E., Halligan, K.W., Tanner, S.D., 1988. Nonspectroscopic interelement interferences in inductively coupled plasma mass spectrometry. *Anal. Chem.* 60, 1472–1474.
- Graney, J.R., Halliday, A.N., Keeler, G.J., Nriagu, J.O., Robbins, J.A., Norton, S.A., 1995. Isotopic record of lead pollution in lake sediments from the northeastern United States. *Geochim. Cosmochim. Acta* 59 (9), 1715–1728.
- Halliday, A.N., Christensen, J.N., Lee, D.-C., Hall, C.M., Luo, X., Rehkämper, M., 2000. Multiple-collector inductively coupled plasma mass spectrometry. In: Barshick, C.M., Duckworth, D.C., Smith, D.H. (Eds.), *Inorganic Mass Spectrometry: Fundamentals and Applications*. Marcel Dekker, New York, pp. 291–328.
- Hamelin, B., Manhès, G., Albarède, F., Allègre, C.J., 1985. Precise lead isotope measurements by the double spike technique: a reconsideration. *Geochim. Cosmochim. Acta* 49, 173–182.
- Hamelin, B., Ferrand, J.L., Alleman, L., Nicholas, E., Véron, A.J., 1997. Isotopic evidence of pollutant lead transport from North America to the subtropical North Atlantic gyre. *Geochim. Cosmochim. Acta* 61, 4423–4428.
- Hirata, T., 1996. Lead isotopic analysis of NIST standard reference materials using multiple collector-inductively coupled plasma mass spectrometry coupled with modified external correction method for mass discrimination effect. *Analyst* 121, 1407–1411.
- Horlick, G., Montaser, A., 1998. Analytical characteristics of ICP-MS. In: Montaser, A. (Ed.), *Inductively Coupled Plasma Mass Spectrometry*. Wiley-VCH, New York, pp. 503–588.
- Kraus, K.A., Moore, G.E., 1953. Anion exchange studies: VI. The divalent transition elements manganese to zinc in hydrochloric acid. *J. Am. Chem. Soc.* 75, 1460–1462.
- Longerich, H.P., Fryer, B.J., Strong, D.F., 1987. Determination of lead isotope ratios by inductively couple plasma-mass spectrometry (ICP-MS). *Spectrochim. Acta* 42B (1–2), 39–48.
- Marcantonio, F., Zimmermann, A., Xu, Y.F., Canuel, E., 2002. A Pb isotope record of mid-Atlantic US atmospheric Pb emissions in Chesapeake Bay sediments. *Mar. Chem.* 77 (2–3), 123–132.
- Maréchal, C., Télouk, P., Albarède, F., 1999. Precise analysis of Cu and Zn isotopic compositions by plasma-source mass spectrometry. *Chem. Geol.* 156, 251–273.
- Montaser, A., 1998. *Inductively Coupled Plasma Mass Spectrometry*. Wiley, New York.
- Niu, H., Houk, R.S., 1996. Fundamental aspects of ion extraction in inductively coupled plasma mass spectrometry. *Spectrochim. Acta* 51B, 779–815.
- Nriagu, J.O., Pacyna, J.M., 1988. Quantitative assessment of worldwide contamination of air, water, and soils by trace metals. *Nature* 333, 134–139.
- Rehkämper, M., Halliday, A., 1998. Accuracy and long-term reproducibility of lead isotopic measurements by multiple-collector inductively coupled plasma mass spectrometry using an external method for correction of mass discrimination. *Int. J. Mass Spectrom.* 181, 123–133.
- Rehkämper, M., Mezger, K., 2000. Investigation of matrix effects for Pb isotope ratio measurements by multiple collector ICP-MS: verification and application of optimized analytical protocols. *J. Anal. At. Spectrom.* 15, 1451–1460.
- Reuer, M.K., Boyle, E.A., Cole, J.E., 2003. A mid-twentieth century reduction in tropical upwelling inferred from coralline trace element proxies. *Earth Planet. Sci. Lett.* 210, 437–452.
- Rosman, K.J.R., Chisholm, W., Boutron, C.F., Candelone, J.-P., Görlach, U., 1993. Isotopic evidence for the source of lead in Greenland snows since the late 1960s. *Nature* 362, 333–335.
- Rosman, K.J.R., Ly, C., Van de Velde, K., Boutron, C.F., 2000. A two century record of lead isotopes in high altitude Alpine snow and ice. *Earth Planet. Sci. Lett.* 176, 413–424.
- Russell, W.A., Papanastassiou, D.A., Tombrello, T.A., 1978. Ca isotope fractionation on the Earth and other solar system materials. *Geochim. Cosmochim. Acta* 42, 1075–1090.
- Shen, G.T., Boyle, E.A., 1987. Lead in corals: reconstruction of historical industrial fluxes to the surface ocean. *Earth Planet. Sci. Lett.* 82, 289–304.
- Shen, G.T., Boyle, E.A., 1988a. Determination of lead, cadmium, and other trace metals in annually-banded corals. *Chem. Geol.* 97, 47–62.
- Shen, G.T., Boyle, E.A., 1988b. Thermocline ventilation of anthropogenic lead in the western North Atlantic. *J. Geophys. Res.* 93 (C12), 15715–15732.
- Sherrell, R.M., Boyle, E.A., Hamelin, B., 1992. Isotopic equilibration between dissolved and suspended particulate lead in the Atlantic Ocean: evidence from ²¹⁰Pb and stable Pb isotopes. *J. Geophys. Res.* 97 (7), 11257–11268.
- Shirahata, H., Elias, R.W., Patterson, C.C., Koide, M., 1980. Chronological variations in concentrations and isotopic compositions of anthropogenic atmospheric lead in sediments of a remote subalpine pond. *Geochim. Cosmochim. Acta* 44, 149–162.
- Shotyk, W., Weiss, D., Appleby, P.G., Cheburkin, A.K., Frei, R., Gloor, M., Kramers, J.D., Reese, S., Van Der Knaap, W.O., 1998. History of atmospheric lead deposition since 12,370 ¹⁴C yr BP from a peat bog, Jura Mountains, Switzerland. *Science* 281, 1635–1640.
- Strelow, F.W.E., 1978. Distribution coefficients and anion exchange behavior of some elements in hydrobromic–nitric acid mixtures. *Anal. Chem.* 50 (9), 1359–1361.

- Sturges, W.T., Barrie, L.A., 1987. Lead 206/207 isotope ratios in the atmosphere of North America as tracers of US and Canadian emissions. *Nature* 329, 144–146.
- Thirlwall, M.F., 2000. Inter-laboratory and other errors in Pb isotope analysis investigated using a $^{207}\text{Pb}/^{204}\text{Pb}$ double spike. *Chem. Geol.* 163, 299–322.
- Thirlwall, M.F., 2001. Inappropriate tail corrections can cause large inaccuracy in isotope ratio determination by MC-ICP-MS. *J. Anal. At. Spectrom.* 16, 1121–1125.
- Thirlwall, M.F., 2002. Multicollector ICP-MS analysis of Pb isotopes using a ^{207}Pb – ^{204}Pb double spike demonstrates up to 400 ppm/amu systematic errors in Tl-normalization. *Chem. Geol.* 184 (3–4), 255–279.
- Todt, W., Cliff, R.A., Hanser, A., Hofmann, A.W., 1996. Evaluation of a ^{202}Pb – ^{205}Pb double spike for high-precision lead isotope analysis. *Geophys. Monogr.* 95, 429–437.
- Turner, P.J., Merren, T.O., Speakman, J., Haines, R.C., Palacz, Z., Meffan-Main, S., 2000. Ion optics of multi-collector ICP-MS systems for precise and accurate isotope ratio measurements. Micromass UK, Manchester.
- United States Bureau of Mines, 1983. *Minerals Yearbook*, vol. 2. US Government Printing Office, Washington.
- Véron, A.J., Church, T.M., Flegal, A.R., Patterson, C.C., Erel, Y., 1993. Response of lead cycling in the surface Sargasso Sea to changes in tropospheric input. *J. Geophys. Res.* 98, 18269–18276.
- Véron, A.J., Church, T.M., Patterson, C.C., Flegal, A.R., 1994. Use of stable lead isotopes to characterize the sources of anthropogenic lead in North Atlantic surface waters. *Geochim. Cosmochim. Acta* 58 (15), 3199–3206.
- Vink, S., Boyle, E.A., Measures, C.I., Yuan, J., 2000. Automated high resolution determination of the trace elements iron and aluminum in the surface ocean using a towed Fish coupled to flow injection analysis. *Deep-Sea Res.* 47, 1141–1156.
- Walder, A.J., 1997. Advanced isotope ratio mass spectrometry II: Isotope ratio measurements by multiple collector inductively coupled plasma mass spectrometry. In: Platzner, I.T., Habfast, K., Walder, A.J., Goetz, A. (Eds.), *Modern Isotope Ratio Mass Spectrometry*. Wiley, New York, pp. 83–108.
- Walder, A.J., Freedman, P.A., 1992. Isotopic ratio measurement using a double focusing magnetic sector mass analyzer with an inductively coupled plasma as an ion source. *J. Anal. At. Spectrom.* 7, 571–575.
- Weiss, D., Shoty, W., Appleby, P.G., Kramers, J.D., Cheburkin, A.K., 1999. Atmospheric Pb deposition since the Industrial Revolution recorded by five Swiss peat profiles: enrichment factors, fluxes, isotopic composition, and sources. *Environ. Sci. Technol.* 33 (9), 1340–1352.
- Weiss, D., Boyle, E.A., Chavagnac, V., Herwegh, M., Wu, J., 2000. Determination of lead isotope ratios in seawater by quadrupole inductively couple plasma mass spectrometry after $\text{Mg}(\text{OH})_2$ co-precipitation. *Spectrochim. Acta* 55B, 363–374.
- White, W.M., Albarède, F., Télouk, P., 2000. High-precision analysis of Pb isotope ratios by multiple collector ICP-MS. *Chem. Geol.* 167, 257–270.
- Woodhead, J.D., Volker, F., McCulloch, M.T., 1995. Routine lead isotope determinations using a lead-207–lead-204 double spike: a long-term assessment of analytical precision and accuracy. *Analyst* 120, 35–39.
- Wu, J., Boyle, E.A., 1997a. Lead in the western North Atlantic Ocean: Completed response to leaded gasoline phaseout. *Geochim. Cosmochim. Acta* 61 (15), 3279–3283.
- Wu, J., Boyle, E.A., 1997b. Low blank preconcentration technique for the determination of lead, copper, and cadmium in small-volume seawater samples by isotope dilution ICP-MS. *Anal. Chem.* 69 (13), 2464–2470.
- York, D., 1966. Least-squares fitting of a straight line. *Can. J. Phys.* 44, 1079–1086.